Investigation of Phase-Modulator-Based All-Optical Bandpass Microwave Filter

Fei Zeng, *Student Member, IEEE, Member, OSA,* and Jianping Yao, *Senior Member, IEEE, Member, OSA*

***Abstract*—Theoretical analysis and experimental implementation of an all-optical bandpass microwave filter are presented. Bandpass filtering is implemented using an electrooptic phase modulator combined with a dispersive device to eliminate the baseband resonance of a typical low-pass filter. In addition to bandpass operation, the proposed filter also provides an improved mainlobe-to-sidelobe ratio (MSR) and a reduced mainlobe bandwidth compared with those of the conventional microwave filters with windowing. A four-tap bandpass microwave filter with a 3-dB mainlobe bandwidth of 2.65 GHz and an MSR of 30 dB is demonstrated. The filter performances, including the reconfigurability, tunability, and the dynamic range, are also discussed.**

***Index Terms*—Bandpass filter, chromatic dispersion, mainlobe-to-sidelobe ratio (MSR), 1-dB compression point, phase modulation.**

I. Introduction

THE USE of photonic devices to implement flexible filters for the processing of microwave and radio-frequency (RF) signals has been an interesting topic for a few years [1], [2]. Compared with the conventional electronic microwave filters, the all-optical microwave filters have many advantages, such as broad bandwidth, low loss, light weight, large tunability, and the immunity to electromagnetic interference. In addition, all-optical microwave filters are of particular interest for applications such as radio-over-fiber (RoF) systems and optically controlled phased-array antennas, where the signals can be processed directly in the optical domain without the need of optical–electrical (O/E) and electrical–optical (E/O) conversions.

Various configurations have been proposed for the implementation of all-optical microwave filters [3]–[8]. However, most reported approaches are based on incoherent operation, in which only the intensity of the optical signal can be manipulated, and hence negative taps are difficult to obtain. This results in a severe limitation on the functionalities of the all-optical filters. For example, bandpass or high-pass filtering cannot be implemented if only positive taps are available. Although in a coherent system the optical phase can be manipulated to achieve negative coefficients [9], [10], the implementation of such a coherent optical signal processor is hindered by the precise control of the optical phase, which is extremely sensitive to the environment variations. Moreover, the maximum time delay has to be shorter than the coherent length of the light source, which further imposes difficulties in the filter fabrication based on fiber optics.

Manuscript received September 22, 2004; revised December 22, 2004.

The authors are with the Microwave Photonics Research Laboratory, School of Information Technology and Engineering, University of Ottawa, Ottawa, ON K1N 6N5, Canada (e-mail: jpyao@site.uottawa.ca).

Digital Object Identifier 10.1109/JLT.2005.844499

To overcome this limitation, several techniques have been proposed to realize negative coefficients and consequently achieve bandpass filtering using incoherent sources. One approach proposed by Sales *et al.* [11] is to use differential detection, which requires converting the optical signal to an electrical signal at the cost of increased system complexity. Other approaches with negative coefficients include wavelength conversion based on cross-gain saturation modulation in a semiconductor optical amplifier (SOA) [12] and carrier depletion effect in a Fabry–Pérot (FP) laser diode [13] or in a distributed-feedback (DFB) laser diode [14]. More recently, Capmany *et al.* [15] proposed a bandpass filter that employed two electrooptic modulators (EOMs). Negative coefficients were obtained by biasing the two EOMs at different operation points. Mora *et al.* [16] presented a simple approach to realizing transversal filters with negative coefficients. The negative taps were obtained by use of the transmission of a broad-band source through uniform Bragg gratings. Chan *et al.* [17] presented a two-tap notch filter with one negative tap, in which a dual-output EOM was used. The EOM was connected in a way such that it undergoes a double-pass modulation. In these configurations, complicated structures or extra active or passive components are required.

In addition, the mainlobe-to-sidelobe ratio (MSR) and the mainlobe bandwidth are other two important issues that must be considered in the filter design. Although it is known from filter theory, uniform taps provide an MSR that increases linearly with the number of taps. This may be insufficient for certain applications, where the available taps are limited. Different weighting functions have been proposed for the MSR improvement, either by adjusting the power of the optical sources [18], [19] or by controlling the attenuation/gain of the taps. However, for a fixed number of taps, the reduction of the MSR by use of appropriate window functions is achieved at the cost of an increased mainlobe bandwidth, which is usually unwanted for many applications.

Recently, we have proposed a method to implement all-optical microwave bandpass filters [20]. It is different from the negative-coefficient bandpass filters discussed in [12]–[17]; the proposed bandpass filter eliminates the baseband resonance of a typical low-pass filter by use of a phase modulator combined with a dispersive device. The fundamental concept was demonstrated based on a simple two-tap filter [20]. However, many issues such as the MSR, mainlobe bandwidth, tunability, and dynamic range were not discussed in [20].

This paper presents a detailed theoretical and experimental investigation on these issues. A bandpass filter with four taps is implemented. It shows that the proposed filter provides simultaneously a lower MSR and a narrower mainlobe bandwidth

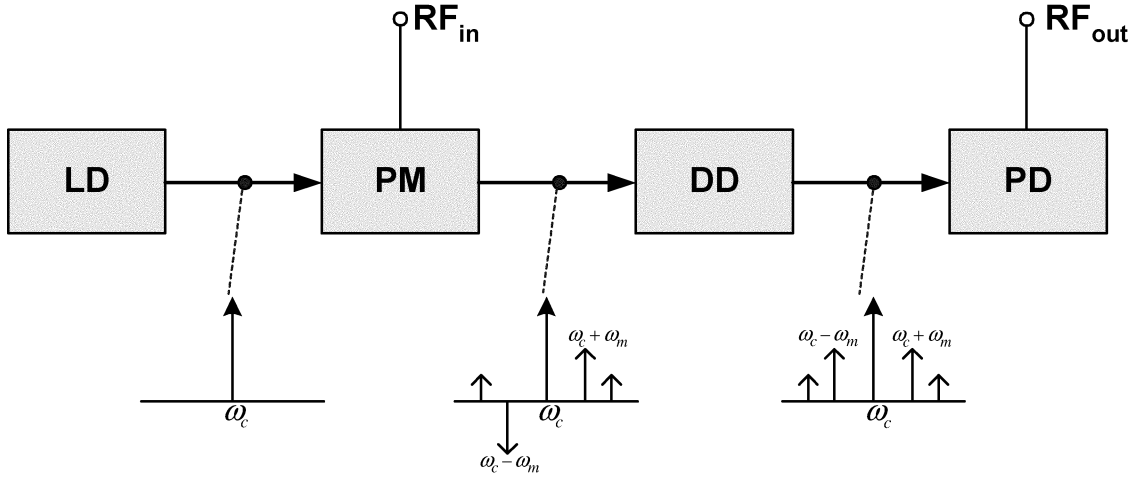

Fig. 1. Diagram of narrow-band phase modulation with intensity detection. LD: Laser diode; PM: phase modulator; DD: dispersion device; PD: photodetector.

compared with the conventional negative-coefficient filters. The performances such as the reconfigurability, tunability, and the dynamic range are also discussed in this paper.

This paper is organized as follows. In Section II, the principle of the phase-modulation-based all-optical bandpass microwave filter is discussed. A theoretical model based on narrow-band phase modulation with intensity detection is developed. Issues such as the MSR and mainlobe bandwidth are discussed. In Section III, experimental implementation of a four-tap bandpass microwave filter is performed to verify the theoretical analysis. Discussions on the filter tunability and the dynamic range are presented in Section IV. A conclusion is drawn in Section V.

II. Theory

Consider a fiber link composed of a single-frequency laser source, an electrooptic phase modulator (EOPM), a dispersive device, and a square-law photodetector. The diagram of the link is shown in Fig. 1, where the laser is fiber coupled to the phase modulator, which is driven by a single-frequency sinusoidal electrical signal; the phase-modulated optical signal is then applied to the dispersive device, and the output is detected by the photodiode. The optical amplitude spectra at different points in the link are schematically shown in Fig. 1.

The normalized amplitude of the phase-modulated optical field $E(t)$ can be expressed in the form of

$$E(t) = \cos\left[\omega_c t + \Delta\varphi(t)\right] = \cos\left[\omega_c t + m_p \cdot V\cos(\omega_m t)\right] \tag{1}$$

where ω_c is carried angular frequency, ω_m is modulating angular frequency, $\Delta\varphi$ is the phase change of the carrier, V is the amplitude of modulating signal, and $m_p = \Delta\varphi_{\max}/V$ is the phase modulation index. Equation (1) can be expanded in terms of Bessel functions of the first kind

$$E(t) = \sum_{n=-\infty}^{\infty} J_n(m_p V)\cdot\cos\left[(\omega_c + n\omega_m)t + \frac{1}{2}n\pi\right] \tag{2}$$

where $J_n(\bullet)$ denotes the nth-order Bessel function of the first kind. To simplify, the argument (m_pV) will be omitted in the following text. From (2), we can see that the phase modulation process generates a series of sidebands with Bessel function amplitude coefficients. The power intensity of each sideband, plotted as the function of m_pV in Fig. 2, is proportional to the square of the coefficient of the corresponding term in (2).

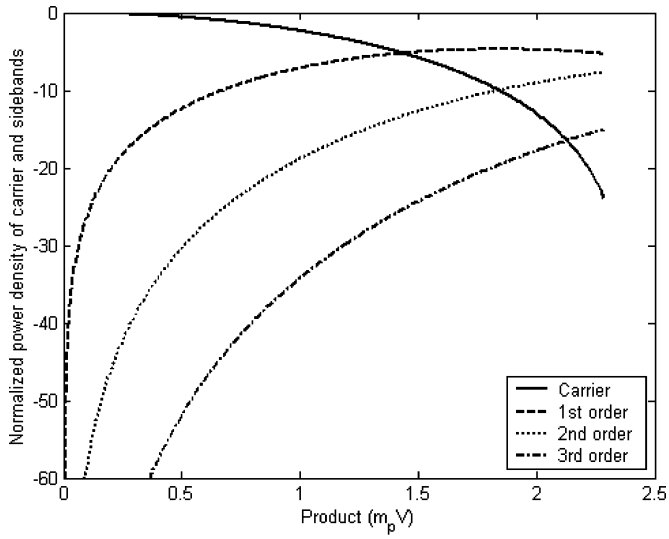

Fig. 2. Normalized power intensities of the carrier and the sidebands as the function of the product m_pV.

From Fig. 2, we see that when m_pV is small, only the first-order upper and lower sidebands can be considered, and higher order sidebands are negligible. If m_pV is relatively large and the power levels of the higher order sidebands are comparable to those of the carrier and the first-order sidebands, the modulation is nonlinear, which imposes a crucial limitation on the dynamic range of the proposed filter. The discussion on dynamic range will be presented in Section IV. Here, under small-signal conditions, the phase modulation can be regarded as a narrow-band linear modulation. Equation (2) can be further simplified as

$$E(t) = J_0\cos(\omega_c t) + J_1\cos\left[(\omega_c+\omega_m)t + \frac{\pi}{2}\right] + J_{-1}\cos\left[(\omega_c-\omega_m)t - \frac{\pi}{2}\right]. \tag{3}$$

Based on the property of Bessel functions, we have

$$J_n = -J_{-n}, \quad \text{when } n \text{ is odd.} \tag{4}$$

We can conclude that the two sidebands are π out of phase at the output of the phase modulator, which is different from an intensity modulation where the two sidebands are in phase. If this signal is directly detected using a photodiode, the radio-frequency (RF) signal cannot be recovered because the beating between the carrier and upper sideband exactly cancels the beating between the carrier and the lower sideband. However, as shown in Fig. 1, if the modulated optical signal passes through a dispersive device, the optical field can be expressed as

$$E(t) \propto J_0 \cos(\omega_c t + \varphi_0) + J_1 \cos\left[(\omega_c + \omega_m)t + \frac{\pi}{2} + \varphi_1\right] - J_1 \cos\left[(\omega_c - \omega_m)t - \frac{\pi}{2} + \varphi_2\right] \quad (5)$$

where φ_0, φ_1, and φ_2 are the phase delays of the spectral components ω_c, $\omega_c + \omega_m$, and $\omega_c - \omega_m$ induced by the chromatic dispersion of the dispersive device. Since the phase delays are different for the three components, which implies that the phase difference of the two sidebands can be effectively rotated to be totally or partially in phase, then the modulating RF signal may be recovered when this dispersed optical signal is fed to the photodetector.

It is well known that the phase delay can be given by an expansion in a Taylor series of the frequency-dependent propagation constant $\beta(\omega)$ and light absorbed by the photodetector generates a current proportional to the square of the optical field [21], [22]. Taking only the RF signal centered at the modulation frequency ω_m and ignoring the dc current and higher order harmonics, we obtain the amplitude of the recovered RF signal

$$E_{\mathrm{RF}}(t) \propto \cos\left(\frac{\varphi_1 + \varphi_2}{2} - \varphi_0\right) \cdot \cos\left(\omega_m t + \frac{\varphi_1 - \varphi_2}{2}\right) = \cos\left(\frac{\pi \chi \lambda_0^2 f_m^2}{c} + \frac{\pi}{2}\right) \cdot \cos(\omega_m t + \theta) \quad (6)$$

where c is the optical wave propagation velocity in free space, χ is the accumulated dispersion of the dispersive device, λ_0 is the central wavelength of the carrier, f_m is the frequency of the modulation signal, and θ is the phase delay of the recovered microwave signal, which is also determined by χ and f_m. The frequency response of this narrow-band phase modulation and intensity-detection operation is shown in Fig. 3. As can be seen, a notch is observed at the dc frequency; the first peak and the second notch can be determined by letting $\pi \chi \lambda_0^2 f_m^2 / c = \pi/2$ and π, respectively.

Now we use an array of N laser sources to replace the single laser source. Assume that the laser sources are not correlated. The central wavelengths are $\lambda_n (n = 1, 2, \cdots, N)$, and the output powers are $P_n (n = 1, 2, \cdots, N)$. As shown in Fig. 4, the combined outputs of the N wavelengths from the laser array are applied to the phase modulator, and the modulated optical signal passes through the dispersive device. The modulating RF signal is recovered at the photodetector, which can be expressed as the summation of resulting electrical signals from the N carriers

$$E_{\mathrm{RF}}(t) \propto \sum_{n=1}^{N} \cos\left(\frac{\pi \chi_n \lambda_n^2 f_m^2}{c} + \frac{\pi}{2}\right) \cdot P_n \cdot \cos(2\pi f_m t + \theta_n) \quad (7)$$

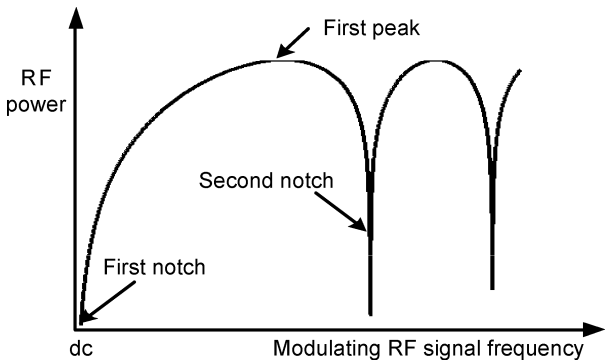

Fig. 3. Recovered RF power versus RF frequency.

where χ_n is the accumulated dispersion for the nth carrier, and θ_n is the phase delay for the nth recovered RF signal.

If the wavelength spacing between any adjacent laser diodes is identical and small, the first term on the right-hand side of (7) can be considered identical for all the wavelengths. Then, (7) can be rewritten as

$$E_{\mathrm{RF}}(t) \propto \cos\left(\frac{\pi \overline{\chi_n} \cdot \overline{\lambda_n}^2 f_m^2}{c} + \frac{\pi}{2}\right) \cdot \sum_{n=1}^{N} P_n \cdot \cos\left[2\pi f_m t + \theta_1 + 2\pi f_m (n-1) T\right] \quad (8)$$

where $\overline{\chi_n}$ and $\overline{\lambda_n}$ denote the average accumulated dispersion and the mean value of carrier wavelength, $T = \overline{\chi_n} \cdot \Delta\lambda$ is the time interval between any two adjacent taps. Applying Fourier transform to both sides of (8), we get the frequency response

$$H(\omega) \propto \underbrace{\cos\left(\frac{\pi \overline{\chi_n} \overline{\lambda_n}^2 f_m^2}{c} + \frac{\pi}{2}\right)}_{H_1(\omega)} \cdot \underbrace{\sum_{n=1}^{N} P_n \cdot \exp\left[j 2\pi f_m (n-1) T\right]}_{H_2(\omega)} \quad (9)$$

where $H_1(\omega)$ represents the dispersion-induced frequency response, and $H_2(\omega)$ is nothing but a frequency response of a typical transversal all-optical low-pass filter. The effective transfer function of this phase-modulation-based microwave filter can be expressed as the multiplication of these two responses, or in other words, a conventional low-pass response $H_2(\omega)$ with a free spectral range (FSR) of $1/T$ is reshaped by the frequency response $H_1(\omega)$.

Based on the above theoretical analysis, a four-tap all-optical bandpass microwave filter is simulated, in which four carriers with $\overline{\lambda_n} = 1570$ nm and wavelength spacing $\Delta\lambda = 0.195$ nm are applied as the light sources. The accumulated dispersion $\chi = 425$ ps/nm at 1570 nm is chosen to ensure the second resonance peak of $H_2(\omega)$ located exactly at the same position of the first peak of $H_1(\omega)$. The frequency response of the proposed microwave filter is shown in Fig. 5. As can be easily seen that the baseband resonance of the low-pass filtering function due to the conventional intensity-modulation direct-detection (IM-DD) scheme is eliminated, and an equivalent bandpass microwave filter is consequently achieved.

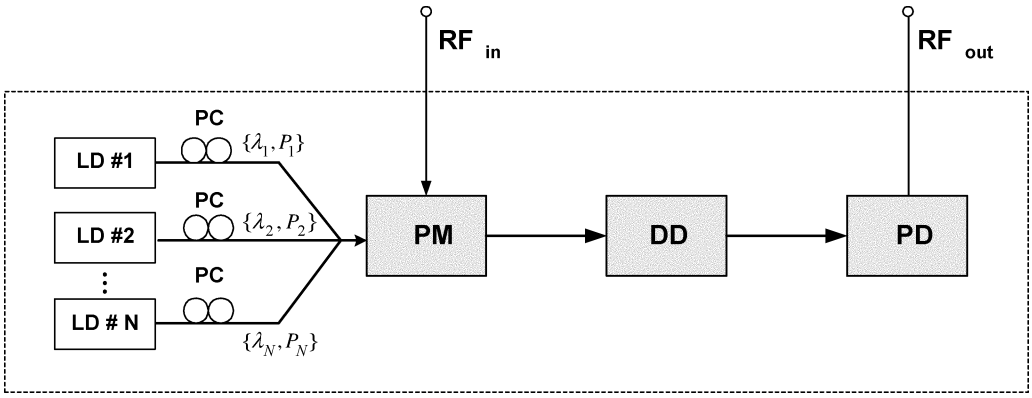

Fig. 4. Diagram of phase-modulator-based all-optical bandpass microwave filter. PC: Polarization controller.

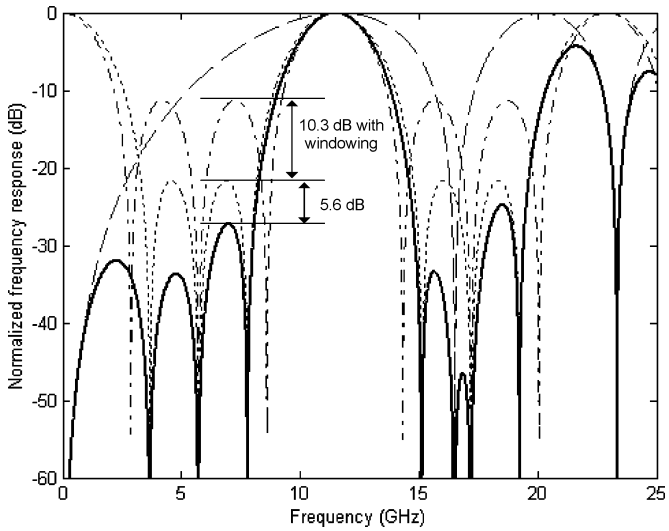

Fig. 5. Simulation results of a four-tap bandpass microwave filter. Dashed–dotted line: $H_2(\omega)$ based on a rectangular window {1, 1, 1, 1}; dotted line: $H_2(\omega)$ based on a Kaiser window {0.54, 1, 1, 0.54}; dashed line: dispersion effects induced $H_1(\omega)$; and solid line: $H(\omega)$ based on the Kaiser window {0.54, 1, 1, 0.54}.

A rectangular window of $\{P_n\} = \{1, 1, 1, 1\}$ and a Kaiser window of $\{P_n\} = \{0.54, 1, 1, 0.54\}$ are applied to show the MSR suppression due to different tap-weight apodization. Compared with the frequency response of a low-pass filter with uniform taps, 10.3-dB MSR improvement is obtained when the Kaiser window is applied, which is at the cost of a 0.4-GHz expansion of 3-dB passband width. However, by use of our approach, an MSR improvement of 15.9 dB can be achieved. Meanwhile, the expansion of the mainlobe bandwidth due to the application of the Kaiser window is only 0.1 GHz, which means that the presented approach makes it possible to improve the MSR and reduce the mainlobe bandwidth simultaneously.

III. Experiment

First, an experiment based on the configuration shown in Fig. 1 is carried to verify the dispersion effects in the phase-modulated optical link. A tunable laser with a tunable range from 1520 to 1620 nm is used as the optical source. A 25-km standard SMF-28 fiber coil is employed as the dispersive device. The fiber shows a chromatic dispersion of 17.9 ps/(nm.km) at 1568 nm, which provides an accumulated dispersion of $\chi = 450$ ps/nm. The frequency response at the output of the photodiode, shown in Fig. 6, is measured by a vector network analyzer by sweeping the modulating frequency from 45 MHz to 25 GHz at the same output power of 3 dBm.

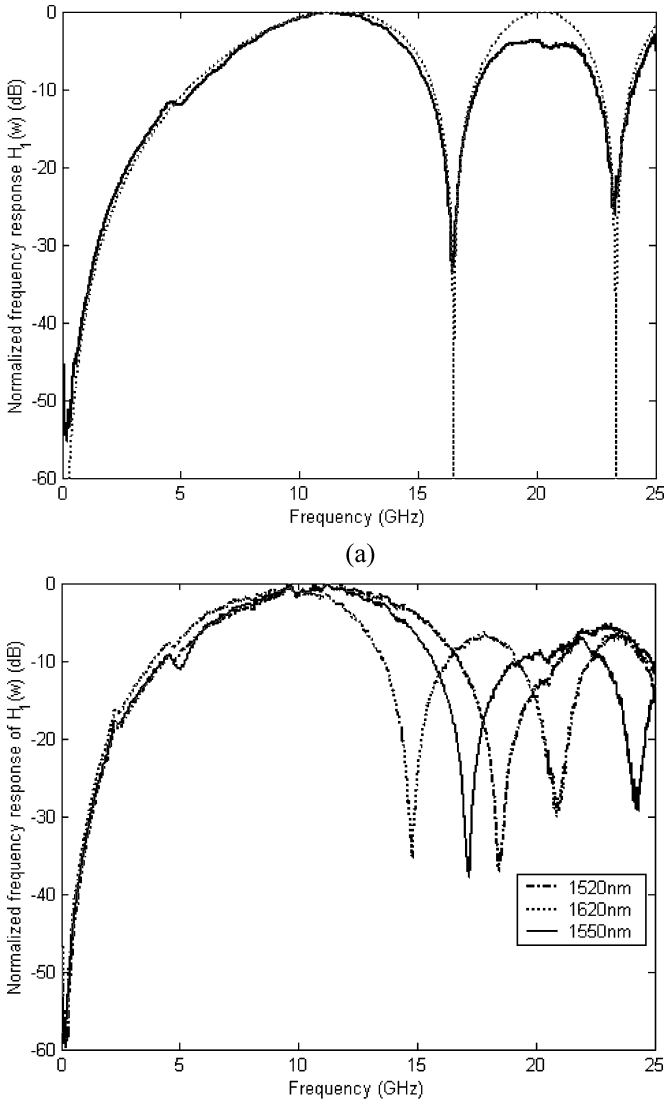

Fig. 6. Measured frequency response of $H_1(\omega)$. (a) Experimental $H_1(\omega)$ (solid) versus theoretical $H_1(\omega)$ (dotted); (b) experimental $H_1(\omega)$ at different carrier wavelengths.

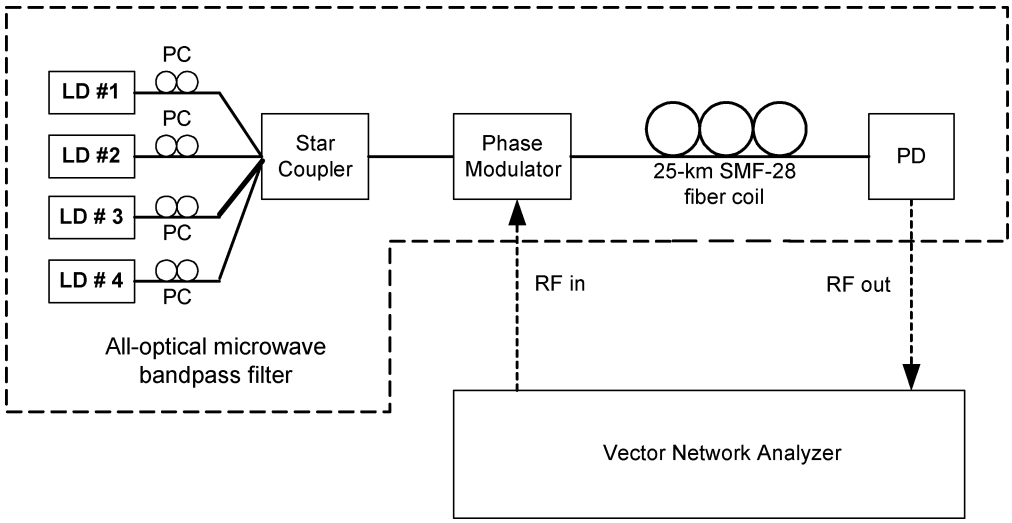

Fig. 7. Experimental setup of the proposed four-tap bandpass microwave filter.

An excellent agreement between the theoretical and experimental results is observed from Fig. 6(a). A quasi-periodic change of the RF power with a notch always at the dc is found. The first peak and the second notch are located at 11.2 and 16.4 GHz, respectively, for $\lambda_0 = 1568.2$ nm. When the central wavelength is tuned around λ_0 by a few nanometers, no obvious change can be observed from the measured $H_1(\omega)$. This verifies the approximation in Section II that $H_1(\omega)$ can be considered identical for all the wavelengths. From Fig. 6(b), we can see that the plot of $H_1(\omega)$ is squeezed or stretched when the carrier wavelength is tuned from 1550 to 1620 or to 1520 nm, respectively. This feature indicates that by varying the carrier frequency or the dispersion of the dispersive medium at large value, the frequency response $H_1(\omega)$ can be tuned. In Section IV, we will show that this feature can be used for filter tuning without introducing any filter response distortion.

The experimental setup of a four-tap all-optical bandpass microwave filter is shown in Fig. 7. Four tunable lasers emitting at wavelengths of $\lambda_1 = 1567.83$ nm, $\lambda_2 = 1568.03$ nm, $\lambda_3 = 1568.23$ nm, and $\lambda_4 = 1568.42$ nm are fed to a high-speed electrooptic phase modulator via a star coupler. The pumping current and polarization state of each laser source are carefully adjusted to obtain a window function of $\{0.54, 1, 1, 0.54\}$ at the output port of the phase modulator, as shown in Fig. 8(a). The same fiber coil is used as the dispersive device. The wavelength spacing between any two adjacent laser diodes is around 0.2 nm, which gives a time delay of 90 ps or an FSR of 11.1 GHz. This FSR ensures that the resonance peak of $H_2(\omega)$ is located at the same position as the first peak of $H_1(\omega)$.

The effective transfer function of the microwave filter $H(\omega)$, shown in Fig. 8(b), is measured using the same vector network analyzer, again an excellent agreement between the theoretical and experimental results are observed. Although the lowest measurement frequency is 45 MHz, it can be extrapolated that the filter response has a notch at the dc frequency and the baseband resonance of the conventional IM-DD-based low-pass filter is eliminated, which indicates clearly the function of an equivalent bandpass filter. As expected, an additional MSR decrease of 4.7 dB and a 3-dB mainlobe bandwidth reduction

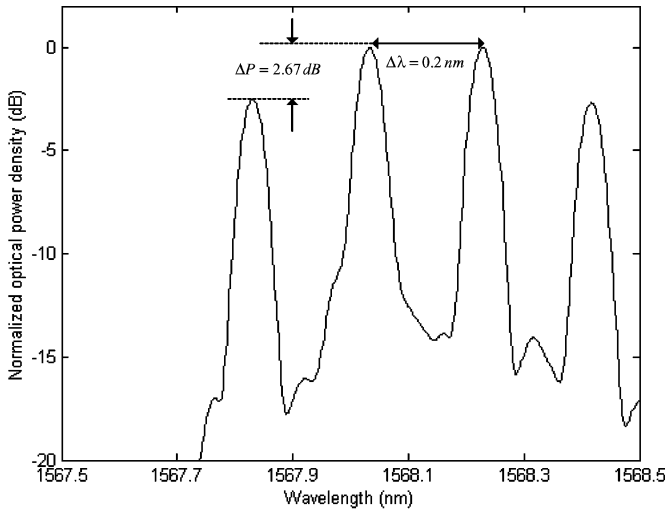

(a)

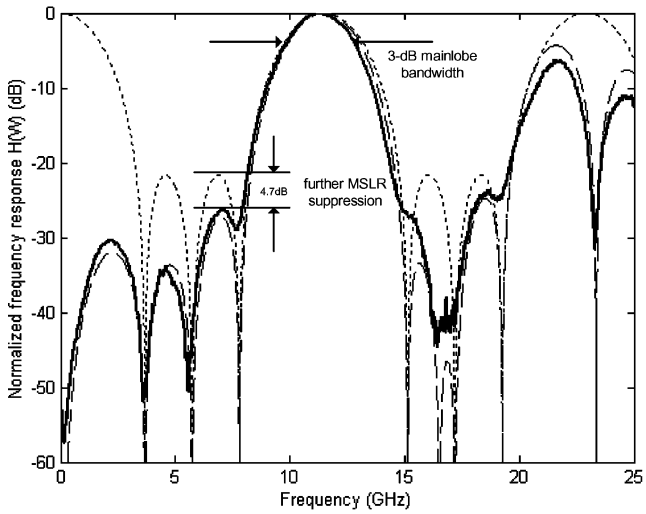

(b)

Fig. 8. Experimental results of the bandpass filter with a window function $\{P_n\} = \{0.54, 1, 1, 0.54\}$. (a) Optical spectrum of the laser array; (b) frequency responses: measured $H(\omega)$ (solid line), theoretical $H(\omega)$ (dashed line), and theoretical $H_2(\omega)$ (dotted line).

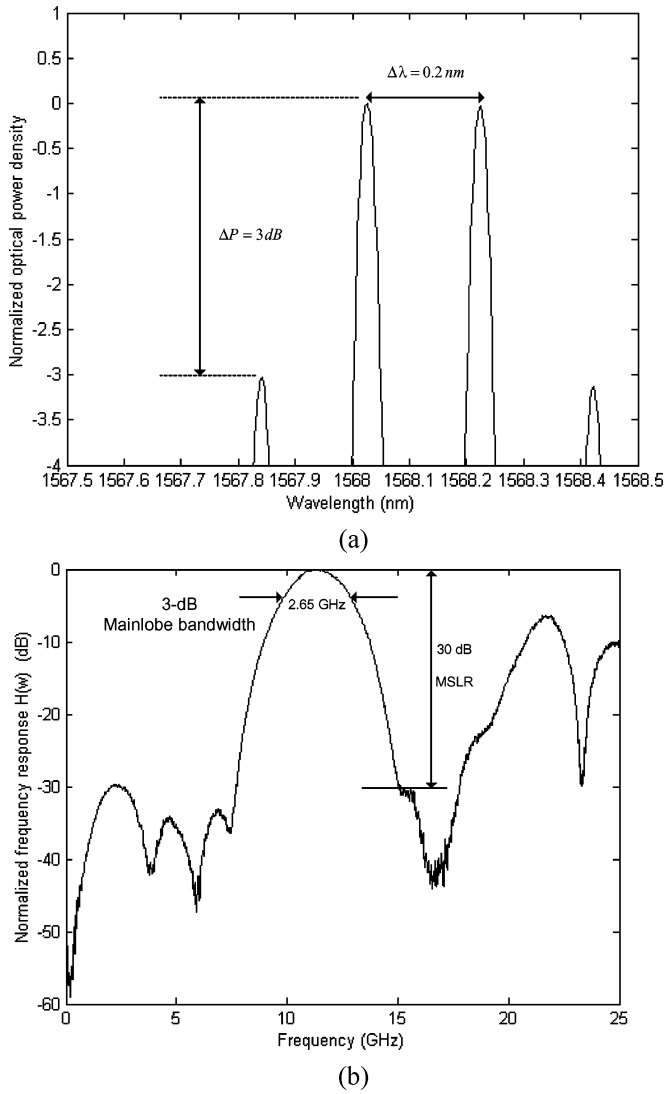

Fig. 9. Experimental results of the bandpass filter with a window function of $\{P_n\} = \{0.50, 1, 1, 0.49\}$. (a) Measured optical spectrum of the laser array, and (b) measured frequency response $H(\omega)$.

of 0.4 GHz are obtained. The degradation of the magnitude response shown at higher frequencies is due to the unflat response of the phase modulator.

Another filter with a different window function of $\{P_n\} = \{0.50, 1, 1, 0.49\}$ is also experimentally implemented to prove the reconfigurability of the proposed bandpass microwave filter. The measured optical power spectrum of the laser sources and the overall frequency response $H(\omega)$ are shown in Fig. 9(a) and (b). A bandpass filter with the passband centered at 11.2 GHz, a 3-dB mainlobe bandwidth of 2.65 GHz, and an MSR of 30 dB is demonstrated.

IV. Further Discussion

A. Tunability

For many applications, the filters are required to be tunable. In order to tune the frequency response of the filter, the time delay T between adjacent taps or the FSR has to be changed. In this approach, the immediate way to tune the filter is to tune the wavelength spacing of the laser array, since the time delay

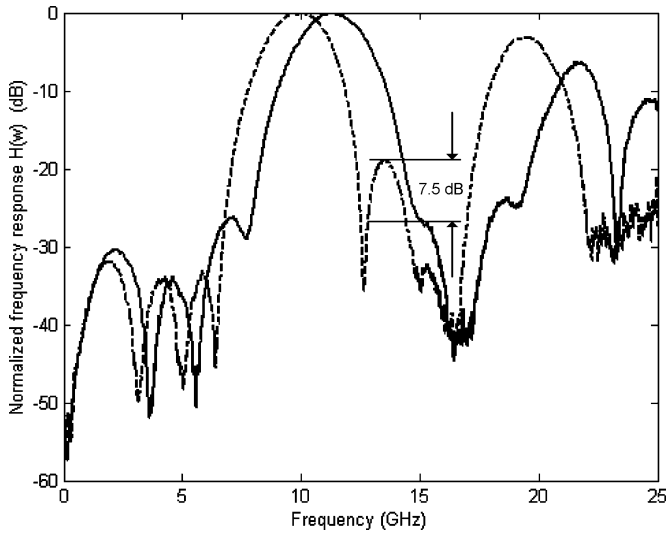

Fig. 10. Frequency responses of the bandpass filter for $\Delta\lambda = 0.2$ nm (solid) and $\Delta\lambda = 0.23$ nm (dashed).

between any two adjacent taps is proportional to the wavelength spacing of these two taps. Fig. 10 shows the filter frequency response when the wavelength spacing between two adjacent laser source is tuned from 0.2 to 0.23 nm. We can see that the central frequency of the passband is changed from 11.2 to 9.7 GHz. However, this tuning is at the cost of the shape distortion of the filter response. As shown in Fig. 10, when the passband is tuned toward a lower frequency, the left-hand-side MSR is further reduced, but the right-hand-side MSR is degraded by about 7.5 dB. The reason is that the small change of wavelength spacing can only lead to the FSR change of $H_2(\omega)$, while $H_1(\omega)$ is almost kept unchanged. As we discussed previously, however, the overall frequency response is the multiplication of $H_1(\omega)$ and $H_2(\omega)$, and the second resonance peak of $H_2(\omega)$ must be located at the same position as the first peak of $H_1(\omega)$ in order to obtain a maximized MSR. Therefore, the MSR is degraded when only $H_2(\omega)$ is changed.

The problem may be solved if a dispersive device with tunable dispersion is used, such as a chirped grating with tunable chirping [23]. By properly changing the dispersion of the dispersive device combined with the tuning of the wavelength spacing of the laser sources, the peak positions of the responses $H_1(\omega)$ and $H_2(\omega)$ can be maintained co-located at the same position; therefore, the filter tuning without any MSR degradation can be achieved.

B. Dynamic Range

Dynamic range is another important factor that needs to be addressed in the filter design. In the earlier analysis in Section II, a small-signal condition is applied to guarantee the linear modulation approximation, for which the second- or higher order sidebands are neglected. However, as shown in Fig. 2, when the modulation depth becomes large, the carrier power level decreases, and the power levels of the sidebands increase quickly, which means for a large dynamic signal, the second- and higher order sidebands need to be considered. The dynamic range here is defined as the range from the minimum discernable signal (lower limit) to the maximum allowable signal (upper limit).

The lower limit is determined by the system-induced noise, such as shot noise from the photodiode and the relative intensity noise from the laser array, which will not be discussed here. The upper limit is determined by the nonlinearity of the phase modulator. In this paper, the 1-dB compression point is introduced to quantify the upper limit. In the analysis, the upper limit is found when the passband peak of the filter frequency response drops by 1 dB from the ideal value.

In general, the recovered RF signal at frequency ω_m can be expressed as the summation of the beatings between any adjacent sidebands [21]

$$E_{\mathrm{RF}}(t) \propto \underbrace{J_0 J_1 \cos\left(\frac{1}{2}\chi_\omega \omega_m^2 + \frac{1}{2}\pi\right)\cdot\cos\left(\omega_m t + \omega_m \cdot \Delta\tau + \frac{1}{3}\dot{\chi}_\omega \omega_m^3\right)}_{\text{beating between the 1st-order sidebands and carrier}} + \underbrace{J_1 J_2 \cos\left(\frac{3}{2}\chi_\omega \omega_m^2 + \frac{1}{2}\pi\right)\cdot\cos\left(\omega_m t + \omega_m \cdot \Delta\tau + \frac{7}{3}\dot{\chi}_\omega \omega_m^3\right)}_{\text{beating between the 1st- and 2nd-order sidebands}} + \cdots \quad (10)$$

where χ_ω denotes the accumulated dispersion in seconds per radian (s/rad), $\dot{\chi}_\omega$ denotes the first-order derivation of χ_ω, and higher order derivations of χ_ω are neglected, and $\Delta\tau$ is the time delay of the RF signal passing through the dispersive device. The beating between the first-order sidebands generates an RF signal at $2\omega_m$, which is not important because it can be filtered out. The Fourier transform of (10) gives the frequency response of $H_1(\omega)$. If $J_1 J_2 \ll J_0 J_1$, the second term on the right-hand side of (10) can be neglected; then, the frequency response $H_1(\omega)$ can be well approximated by (6) and has a frequency response that is independent of the input electrical signal power. When the product $J_1 J_2$ increases, the power level of the recovered RF signal becomes nonlinearly proportional to the power level of the modulating signal. In this case, the phase modulation cannot be approximated as a linear modulation, and the frequency response $H_1(\omega)$ is now power dependent.

Again, the 25-km SMF-28 fiber is used as the dispersion device, which has a dispersion profile given by

$$D_\lambda = \frac{S_0}{4}\left[\lambda - \frac{\lambda_0^4}{\lambda^3}\right] \mathrm{ps/(nm\cdot\ km)} \quad (11)$$

where $\lambda_0 = 1310$ nm is the zero-dispersion wavelength, and $S_0 \leq 0.092\ \mathrm{ps/(nm^2 \cdot km)}$ is the zero-dispersion slope. The phase modulator employed in the experiment has a modulation index m_p of $\pi/4.8$ V at dc. Based on these parameters, the level at the passband peak of the filter frequency response as a function of the input signal power is plotted in Fig. 11.

From Fig. 11, we can see that the input power corresponding to the 1-dB compression point is about 10.3 dBm. This is the upper limit of the dynamic range of this filter. At this point, the product $J_1 J_2$ is around 30 dB lower than $J_0 J_1$, which means that the beating between the carrier and the first-order sidebands is dominant and the beating between the carrier and the higher order sidebands are negligible. When the input signal power further increases, the filter frequency response at the passband peak decreases quickly, and the total frequency response of $H_1(\omega)$ distorts significantly, as shown in Fig. 12.

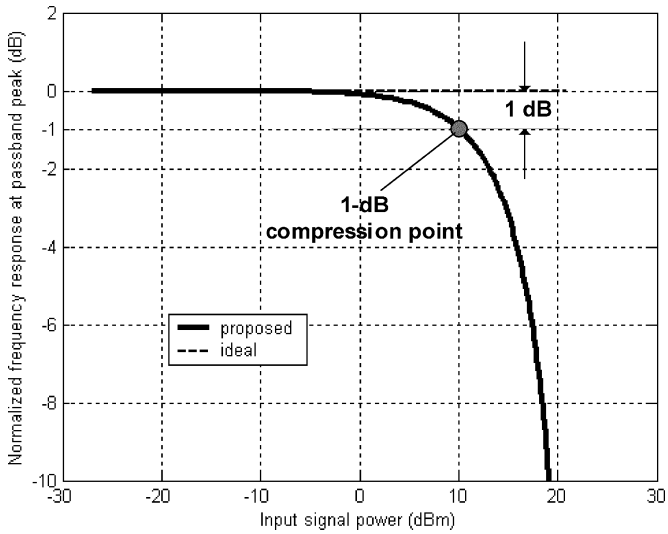

Fig. 11. Frequency response at the passband peak versus input power.

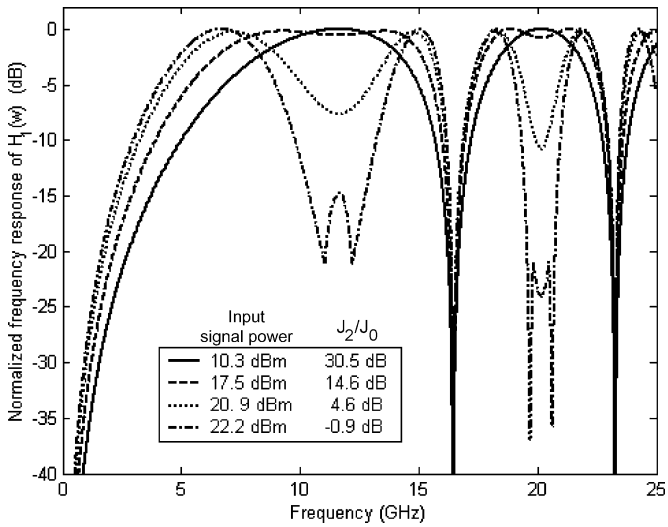

Fig. 12. Frequency responses of $H_1(\omega)$ for different input signal power levels at $m_p = \pi/4.8$ V.

In addition, if the input RF signal contains two frequency components ω_{m1} and ω_{m2}, the phase-modulated optical field can be expressed as

$$E(t) = \sum_{n=-\infty}^{\infty}\sum_{k=-\infty}^{\infty} J_n(m_p V_1)\cdot J_k(m_p V_2) \cdot \cos\left[(\omega_c + n\omega_{m1} + k\omega_{m2})t + \frac{1}{2}n\pi + \frac{1}{2}k\pi\right] \quad (12)$$

where V_1 and V_2 represent the amplitudes of the modulating signal at frequency ω_{m1} and ω_{m2}, respectively. Intermodulation products at $\omega_{m1} + \omega_{m2}$, $2\omega_{m1} + \omega_{m2}$, and $\omega_{m1} + 2\omega_{m2}$ as well as at the multiples of ω_{m1} and ω_{m2} may be generated. However, based on the earlier discussion, if the power levels of the two signals are both below the 1-dB compression point, these components can be neglected, and the proposed bandpass microwave filter is linear.

V. Conclusion

Theoretical analysis and experimental implementation of an all-optical bandpass microwave filter were presented. In the proposed filter structure, an electrooptic phase modulator (EOPM) combined with a dispersive device was employed to eliminate the baseband resonance of a typical low-pass filter. In addition to the simple bandpass operation, the proposed filter has a better performance in terms of the MSR and the mainlobe bandwidth compared with the conventional microwave filters with windowing. A four-tap bandpass microwave filter with a 3-dB mainlobe bandwidth of 2.65 GHz and an MSR of 30-dB was demonstrated. Other issues, including the reconfigurability, tunability, and upper limit of dynamic range, were also discussed. It should be mentioned that due to the employment of a length of single-mode fiber, the output of the proposed filter can be naturally distributed to a remote site, which provides an added advantage to the proposed filter, especially for radio-over-fiber applications. On the other hand, if the proposed filter is only used for local filtering, a dispersion-tunable linearly chirped fiber Bragg grating may be used to replace the fiber link as a dispersive device, and the compactness of the proposed filter can be significantly improved.

References

[1] K. Wilner and A. P. Van Den Heuvel, "Fiber-optic delay lines for microwave signal processing," *Proc. IEEE*, vol. 64, pp. 805–807, 1976.

[2] K. Jackson, S. Newton, B. Moslehi, M. Tur, C. Cutler, J. Goodman, and H. J. Shaw, "Optical fiber delay-line signal processing," *IEEE Trans. Microw. Theory Tech.*, vol. 33, no. 3, pp. 193–204, Mar. 1985.

[3] S. Sampson, R. Griffin, and D. Jackson, "Photonic CDMA by coherent matched filtering using time-address coding in optical ladder networks," *J. Lightw. Technol.*, vol. 12, no. 11, pp. 2001–2010, Nov. 1994.

[4] J. Capmany and J. Cascon, "Discrete time fiber-optic signal processors using optical amplifiers," *J. Lightw. Technol.*, vol. 12, no. 1, pp. 106–117, Jan. 1994.

[5] D. Norton, S. Johns, C. Keefer, and R. Soref, "Tunable microwave filtering using high dispersion fiber time delays," *IEEE Photon. Technol. Lett.*, vol. 6, no. 7, pp. 831–832, Jul. 1994.

[6] D. B. Hunter, R. Minasian, and P. A. Krug, "Tunable optical transversal filter based on chirped gratings," *Electron. Lett.*, vol. 31, pp. 2207–2210, Dec. 1995.

[7] W. Zhang, J. A. R. Williams, and I. Bennion, "Polarization synthesized optical transversal filter employing high birefringence fiber gratings," *IEEE Photon. Technol. Lett.*, vol. 13, no. 5, pp. 523–525, May 2001.

[8] V. Polo, B. Vidal, J. L. Corral, and J. Marti, "Novel tunable photonics microwave filter based on laser arrays and N × N AWG-based delay lines," *IEEE Photon. Technol. Lett.*, vol. 15, no. 4, pp. 584–586, Apr. 2003.

[9] K. Sasayama, M. Okuno, and K. Habara, "Coherent optical transversal filter using silica-based waveguides for high-speed signal processing," *J. Lightw. Technol.*, vol. 9, no. 10, pp. 1225–1230, Oct. 1991.

[10] F. Coppinger, C. K. Madsen, and B. Jalali, "Photonic microwave filtering using coherently coupled integrated ring resonators," *Microw. Opt. Technol. Lett.*, vol. 21, pp. 90–93, Feb. 1999.

[11] S. Sales, J. Capmany, J. Marti, and D. Pastor, "Experimental demonstration of fiber-optic delay line filters with negative coefficients," *Electron. Lett.*, vol. 31, pp. 1095–1096, Jul. 1995.

[12] F. Coppinger, S. Yegnanarayanan, P. D. Trinh, and B. Jalali, "All-optical RF filter using amplitude inversion in a semiconductor optical amplifier," *IEEE Trans. Microw. Theory Tech.*, vol. 45, no. 8, pp. 1473–1477, Aug. 1997.

[13] X. Wang and K. T. Chan, "Tunable all-optical incoherent bipolar delay-line filter using injection-locked Fabry–Perot laser and fiber Bragg gratings," *Electron. Lett.*, vol. 36, pp. 2001–2002, Dec. 2000.

[14] S. Li, K. S. Chiang, W. A. Gambling, Y. Liu, L. Zhang, and I. Bennion, "A novel tunable all-optical incoherent negative-tap fiber-optic transversal filter based on a DFB laser diode and fiber Bragg gratings," *IEEE Photon. Technol. Lett.*, vol. 12, no. 9, pp. 1207–1209, Sep. 2000.

[15] J. Capmany, D. Pastor, A. Martinez, B. Ortega, and S. Sales, "Microwave photonics filters with negative coefficients based on phase inversion in an electro-optic modulator," *Opt. Lett.*, vol. 28, pp. 1415–1417, Aug. 2003.

[16] J. Mora, M. V. Andres, J. L. Cruz, B. Ortega, J. Capmany, D. Pastor, and S. Sales, "Tunable all-optical negative multitap microwave filters based on uniform fiber Bragg gratings," *Opt. Lett.*, vol. 28, pp. 1308–1310, Aug. 2003.

[17] E. H. W. Chan and R. A. Minasian, "Novel all-optical RF notch filters with equivalent negative tap response," *IEEE Photon. Technol. Lett.*, vol. 16, no. 5, pp. 1370–1372, May 2004.

[18] D. B. Hunter and R. A. Minasian, "Microwave optical filters using in-fiber Bragg grating arrays," *IEEE Microw. Guided Wave Lett.*, vol. 6, no. 2, pp. 103–105, Feb. 1996.

[19] J. Capmany, D. Pastor, and B. Ortega, "Efficient sidelobe suppression by source power apodization in fiber optic microwave filters composed of linearly chirped fiber grating by laser array," *Electron. Lett.*, vol. 35, pp. 640–642, Apr. 1999.

[20] F. Zeng and J. P. Yao, "All-optical bandpass microwave filter based on an electro-optic phase modulator," *Opt. Express*, vol. 12, pp. 3814–3819, Aug. 2004.

[21] G. J. Meslener, "Chromatic dispersion induced distortion of modulated monochromatic light employing direct detection," *IEEE J. Quantum Electron.*, vol. 20, no. 10, pp. 1208–1216, Oct. 1984.

[22] H. Schmuck, "Comparison of optical millimeter-wave system concepts with regard to chromatic dispersion," *Electron. Lett.*, vol. 31, pp. 1848–1849, Nov. 1995.

[23] Y. Liu, J. P. Yao, X. Dong, and J. Yang, "Tunable chirping of a fiber Bragg grating without center wavelength shift using simply supported beam," *Opt. Eng.*, vol. 41, pp. 740–741, Apr. 2002.

Fei Zeng (S'04), photograph and biography not available at the time of publication.

Jianping Yao (M'99–SM'01), photograph and biography not available at the time of publication.